JOURNAL OF VIROLOGY, Oct. 2000, p. 9586–9593 Vol. 74, No. 20
0022-538X/00/$04.00+0

Biochemical Characterization of the Equine Arteritis Virus Helicase Suggests a Close Functional Relationship between Arterivirus and Coronavirus Helicases

ANJA SEYBERT,[1] LEONIE C. VAN DINTEN,[2]† ERIC J. SNIJDER,[2] AND JOHN ZIEBUHR[1]*

Institute of Virology and Immunology, University of Würzburg, Würzburg, Germany,[1] and Department of Virology, Center of Infectious Diseases, Leiden University Medical Center, Leiden, The Netherlands[2]

Received 15 June 2000/Accepted 18 July 2000

The arterivirus equine arteritis virus nonstructural protein 10 (nsp10) has previously been predicted to contain a Zn finger structure linked to a superfamily 1 (SF1) helicase domain. A recombinant form of nsp10, MBP-nsp10, was produced in *Escherichia coli* as a fusion protein with the maltose-binding protein. The protein was partially purified by affinity chromatography and shown to have ATPase activity that was strongly stimulated by poly(dT), poly(U), and poly(dA) but not by poly(G). The protein also had both RNA and DNA duplex-unwinding activities that required the presence of 5′ single-stranded regions on the partial-duplex substrates, indicating a 5′-to-3′ polarity in the unwinding reaction. Results of this study suggest a close functional relationship between the arterivirus nsp10 and the coronavirus helicase, for which NTPase and duplex-unwinding activities were recently demonstrated. In a number of biochemical properties, both arterivirus and coronavirus SF1 helicases differ significantly from the previously characterized RNA virus SF1 and SF2 enzymes. Thus, the combined data strongly support the idea that nidovirus helicases may represent a separate group of RNA virus-encoded helicases with distinct properties.

Equine arteritis virus (EAV) is the prototype of the *Arteriviridae*, a family of positive-stranded, enveloped RNA viruses which also includes *Lactate dehydrogenase-elevating virus, Porcine reproductive and respiratory syndrome virus*, and *Simian haemorrhagic fever virus* (for a review, see 47). A common ancestry of the *Arteriviridae* and *Coronaviridae* seems probable (6), and, consequently, the two families have been united in the order *Nidovirales* (3). The phylogenetic relationship between arteri- and coronaviruses is most evident from the organization and expression of their replicase genes. Thus, for example, both arteri- and coronaviruses (i) encode a very similar array of functional domains in their replicase genes, (ii) use ribosomal frameshifting to express key replicative functions, (iii) control the activity of the individual subunits of the viral replication and transcription machinery by extensive proteolytic processing of large protein precursors, and (iv) use a discontinuous transcription mechanism to produce a nested set of subgenomic (sg) mRNAs for structural gene expression (3, 8).

The EAV replicase gene comprises the 5′-terminal three-fourths of the 12.7-kb genome and is composed of two open reading frames (ORFs), ORF1a and ORF1b (6). The upstream ORF1a encodes the ORF1a protein (187 kDa), and ORF1a and ORF1b together encode the ORF1ab protein (345 kDa). Expression of the ORF1b-encoded part of the ORFlab protein involves a ribosomal frameshift in the ORF1a-1b overlap region during translation of the genomic RNA (6). The primary translation products, which are also called replicase polyproteins, are extensively processed by three virus-encoded proteinases to produce 12 mature proteins (nonstructural protein 1 [nsp1] to nsp12), as well as multiple processing intermediates (for a recent review, see 63). To date, specific functions have been assigned to only a few of these proteins. Thus, for example, nsp1, nsp2, and nsp4 harbor proteolytic activities (48–50), and the hydrophobic domains present in nsp2, nsp3, and nsp5 have been found to direct the viral replication and transcription complexes to intracellular membranes of the endoplasmic reticulum and intermediate compartment (40, 52). The ORF1b-encoded part of the ORF1ab protein is believed to contain functions essential for viral RNA replication and sg mRNA transcription (6). Its processing by the nsp4 serine proteinase yields four end products (nsp9 through nsp12), including those that carry the putative RNA-dependent RNA polymerase (nsp9) and nucleoside triphosphatase (NTPase)-helicase (nsp10) activities (54, 56).

Besides the RNA-dependent RNA polymerase domain, the helicase is the most conserved component of the nidovirus RNA synthesis machinery (12–14, 16, 29) and has therefore attracted much attention (53–57). The arterivirus helicase is amino terminally linked to a putative Zn finger structure (6). This combination of a Zn finger structure with a helicase domain is also found in the related coronavirus helicases (7, 17, 23) and a number of cellular and viral helicases (9, 25, 34, 39, 58). Recently, genetic evidence was obtained to show that both the Zn finger itself and the region connecting the Zn finger to the carboxyl proximal part of nsp10 ("hinge spacer") are critically involved in different processes of the EAV life cycle, including genome replication, mRNA transcription, and possibly also virion biogenesis (53, 55, 57).

The arterivirus helicase domain has been classified as belonging to helicase superfamily 1 (SF1) (27). Putative SF1 helicases are extremely widespread among positive-stranded RNA viruses. Based on sequence comparisons, they have also been identified in a variety of plant virus families, as well as alpha-, rubi-, hepatitis E, and coronaviruses (13, 14, 16). Similarly to EAV nsp10, a number of these viral enzymes have been implicated in diverse aspects of transcription and replication but also in RNA stability and cell-to-cell movement (5,

* Corresponding author. Mailing address: Institute of Virology and Immunology, University of Würzburg, Versbacher Str. 7, 97078 Würzburg, Germany. Phone: 49-931-2013966. Fax: 49-931-2013934. E-mail: ziebuhr@vim.uni-wuerzburg.de.

†Present address: Department of Molecular Virology, Institut Jacques-Monod, 75251 Paris Cedex 05, France.

24, 30, 36–38, 41, 44). However, despite their importance, there is very little detailed information on the enzymatic properties of RNA virus SF1 helicases. Only a few proteins have been shown to have NTPase activity, but, in striking contrast to other helicases, the activity of these proteins was not significantly stimulated by homopolynucleotides (18, 23, 26, 42). Furthermore, numerous attempts to detect the predicted RNA duplex-unwinding activity of these proteins have failed. Therefore, the functional assignment of these proteins as true helicases, that is, nucleic acid duplex-unwinding enzymes, has been questioned (27). Only very recently has experimental evidence for duplex-unwinding activity been obtained for two viral proteins of this superfamily (11, 46). The biochemical characterization of one of these proteins, the human coronavirus 229E (HCoV) helicase, revealed that this protein has both RNA and DNA duplex-unwinding activities with a preference for oligopyrimidine-tailed substrates. Furthermore and in obvious contrast to the previously characterized RNA virus SF2 helicases, a 5′-to-3′ polarity of the unwinding reaction has been demonstrated (46).

The helicase domains of the three nidovirus genera, that is, coronaviruses, toroviruses, and arteriviruses, were previously proposed to represent a separate phylogenetic lineage of the RNA virus SF1 helicases (14, 29). It was thus tempting to believe that, despite the differences in their primary structures, the arterivirus nsp10 and coronavirus helicases may have similar functional properties. To test this hypothesis, we expressed and purified EAV nsp10. The subsequent biochemical characterization revealed that the recombinant nsp10 has polynucleotide-stimulated ATPase and both RNA and DNA duplex-unwinding activities. The DNA duplex-unwinding activity was used to show that 5′ single-stranded tails on the partial-duplex substrates were required for unwinding, indicating a 5′-to-3′ polarity of the helicase activity. Taken together, the data are fully consistent with the recently reported coronavirus helicase data but stand in clear contrast to the biochemical properties of RNA virus SF2 helicases.

MATERIALS AND METHODS

Construction of bacterial expression plasmids pMal-nsp10 and pMal-nsp10-KQ. The coding sequence of amino acids 2371 through 2837 of the EAV ORF1ab protein followed by a translation stop codon was amplified by PCR from pL(2371–2837) plasmid DNA (54) and cloned into the *Xmn*I-*Sal*I restriction sites of the bacterial expression vector pMal-c2 (New England Biolabs, Schwalbach, Germany). The upstream PCR primer contained an *Eag*I restriction site that was introduced by replacing the wild-type Ser-2371 codon AGT with TCG, which also encodes Ser. The resulting plasmid, pMal-nsp10, encodes a fusion protein consisting of the maltose-binding protein (MBP) of *Escherichia coli* and full-length EAV nsp10. The plasmid pMal-nsp10-KQ is identical to pMal-nsp10, except for a single-base exchange resulting in the substitution of Gln for Lys-2534 in nsp10.

Protein expression and purification. *E. coli* TB1 bacteria (New England Biolabs) containing either plasmid pMal-nsp10 or pMal-nsp10-KQ were grown at 37°C in Luria-Bertani medium containing 100 μg of ampicillin per ml until they reached a culture density (absorbency at 595 nm ([A_{595}]) of 0.6. The expression of the recombinant proteins was induced by addition of 0.5 mM isopropyl-β-D-thiogalactopyranoside (IPTG). Upon induction, the temperature was shifted to 24°C. The cells were harvested after growing for another 4 h and 30 min, and the cell paste was suspended in column buffer (20 mM Tris-Cl [pH 8.0], 1 M NaCl, 1 mM EDTA, 1 mM EGTA, 1 mM dithiothreitol, 10% glycerol) and disrupted by sonication as described previously (22). Tween 20 (0.1%) was added, and the solution was centrifuged (20,000 × *g*, 30 min) to produce a clear supernatant that was then loaded onto a column packed with amylose resin (New England Biolabs). After extensive washing with column buffer containing 0.1% Tween 20, the proteins were eluted in the same buffer containing 10 mM maltose. Aliquots of the purified proteins were frozen on dry ice and stored at −80°C until needed.

Nucleoside triphosphatase assay. In the ATPase assay, 250 fmol to 4 pmol of the MBP-nsp10 or MBP-nsp10-KQ fusion proteins was incubated in 40 μl of buffer N containing 20 mM HEPES-KOH (pH 7.4), 300 μM ATP, 5 mM magnesium acetate, 2 mM dithiothreitol, 25 μg of bovine serum albumin per ml, and 250 nCi of [γ-^{32}P]ATP (3,000 Ci/mmol). In the GTPase assay, ATP and [γ-^{32}P]ATP were replaced by 300 μM GTP and 250 nCi [γ-^{32}P]GTP (3,000 Ci/mmol), respectively. When included, polynucleotides and polyribonucleotides (5.4 to 8.3 Svedberg units) were at the indicated concentrations of 1, 50, or 150 μg/ml. The reactions were incubated at 30°C for 30 min and stopped by adding EDTA to a final concentration of 100 mM. The samples were analyzed by polyethyleneimine-cellulose thin-layer chromatography with 0.15 M formic acid–0.15 M LiCl (pH 3.0) as the liquid phase. The reaction products were quantified by phosphorimaging of the dried chromatographic plates (ImageQuant software; Molecular Dynamics, Sunnyvale, Calif.).

Preparation of duplex RNA and DNA substrates. For 5′-RNA2, two oligonucleotides, 5′-R2a (5′-CGTTGGCGCGCTAATACGACTCACTATAGGGATC CCTTTAGTGAGGGTTAATTGCGCGCGTTGC-3′) and 5′-R2b (5′-GCAAC GCGCGCAATTAACCCTCACTAAAGGGATCCCTATAGTGAGTCGTAT TAGCGCGCCAACG-3′), were annealed, digested with *Bss*HII, and ligated with the large fragment of *Bss*HII-digested pBluescript II KS(+) DNA. The resultant plasmid was designated pBS-65/66. Next, two oligonucleotides, 5′-R2c [5′-GATC-d(pT)$_{15}$-CTAGAACCGCTGCGGCTGGATCCCG-3′] and 5′-R2d [5′-CGGGATCCAGCCGCAGCGGTTCTAG-d(pA)$_{15}$-GATC-3′], were annealed, digested with *Bam*HI, and ligated with *Bam*HI-digested pBS-65/66. The resultant plasmid was linearized with either *Bam*HI or *Xba*I and used as a template for run-off transcription with either T7 RNA polymerase or T3 RNA polymerase. The T3 transcript was synthesized in the presence of 2 μCi of [α-^{32}P]CTP per μl (800 Ci/mmol).

For 3′-RNA2, two synthetic oligonucleotides, 3′-R2a [5′-CACTCCC-d(pT)$_{15}$-AAA-3′] and 3′-R2b [5′-TTT-d(pA)$_{15}$-GGGAGTGAGCT-3′], were annealed, phosphorylated with T4 polynucleotide kinase, and ligated with the larger fragment of *Sac*I-*Eco*RV-digested pBluescript II KS(+) DNA. The resultant plasmid was linearized with *Dra*I and used as the template for run-off transcription with T7 RNA polymerase. For the preparation of the partially complementary RNA strand, two oligonucleotides, 3′-R2c (5′-CGCGCGTAATACGACTCACTATA GGGAGTGAGCTCCAATTCGCCCGGG-3′) and 3′-R2d (5′-CGCGCCCGG GCGAATTGGAGCTCACTCCCTATAGTGAGTCGTATTACG-3′), were annealed, phosphorylated, and ligated with the larger fragment of *Bss*HII-digested pBluescript II KS(+) DNA. The resultant plasmid was linearized with *Sma*I and used as the template for run-off transcription with T7 RNA polymerase in the presence of 2 μCi of [α-^{32}P]CTP per μl (800 Ci/mmol).

In vitro-transcribed RNA was purified by phenol-chloroform extraction and gel filtration chromatography using Micro Bio-Spin 6 columns (Bio-Rad Laboratories, Munich, Germany). The RNA duplex was produced by annealing a mixture of two RNAs with a 10-fold excess of unlabeled RNA over [α-^{32}P]CTP-labeled RNA in buffer E (25 mM HEPES-KOH[pH 7.4], 500 mM NaCl, 1 mM EDTA, 0.1% [wt/vol] sodium dodecyl sulfate [SDS]). The reaction mixture was denatured for 5 min at 95°C and slowly cooled to room temperature.

To produce duplex DNA substrates, two synthetic oligonucleotides (HPSF quality; MWG-Biotech, Munich, Germany) were annealed as described above. Oligonucleotides were labeled with [γ-^{32}P]ATP (3,000 Ci/mmol) using T4 polynucleotide kinase. The labeled DNA was purified by phenol-chloroform extraction and gel filtration chromatography using Micro Bio-Spin 6 columns.

For DNA-0, the radioactively labeled oligonucleotide DR (5′-GGTGCAGC CGCAGCGGTGCTCG-3′) and oligonucleotide D1 (5′-CGAGCACCGCTGC GGCTGCACC-3′) were annealed. This substrate contained no single-stranded regions. For 5′-3′-DNA-T30, the radioactively labeled oligonucleotide D2 [5′-GGTGCAGCCGCAGCGGTGCTCG-d(pT)$_{30}$-3′] and oligonucleotide D3 [5′-d(pT)$_{30}$-CGAGCACCGCTGCGGCTGCACC-3′] were annealed. This twin-tailed ("forked") substrate contained 5′ and 3′ single-stranded regions on one end of the partial duplex DNA. For 5′-DNA-3′-T30, the radioactively labeled oligonucleotide DR and oligonucleotide D4 [5′-d(pT)$_{30}$-CGAGCACCGCTGC GGCTGCACC-d(pT)$_{30}$-3′] were annealed. This substrate contained 5′ and 3′ single-stranded regions at opposite ends of the partial duplex DNA. For 3′-DNA-T30, the oligonucleotide D1 and the radioactively labeled oligonucleotide D2 were annealed. For 5′-DNA-T30, the radioactively labeled oligonucleotide DR and oligonucleotide D3 were annealed.

Duplex-unwinding assay. MBP-nsp10 or MBP-nsp10-KQ was incubated in a volume of 40 μl with 90 fmol of partial-duplex-RNA or 25 fmol of partial-duplex-DNA substrates for 30 min at 30°C in a buffer containing 20 mM HEPES-KOH (pH 7.4), 5 mM ATP, 10% glycerol, 5 mM magnesium acetate, 2 mM dithiothreitol, and 0.1 mg of bovine serum albumin per ml. The NaCl concentration in the reactions, resulting from substrate and protein storage buffers, was 25 mM. The reactions were stopped by the addition of 10 μl of 5% SDS–15% Ficoll–100 mM EDTA–0.25% bromphenol blue dye. The reaction products were separated on 10 to 20% gradient polyacrylamide–1× TBE gels (acrylamide/bisacrylamide ratio, 19 to 1) at 4 W until the bromophenol blue dye approached the bottom of the gel. The gels were exposed to X-ray film at −70°C.

RESULTS

Bacterial expression and purification of recombinant nsp10 proteins. We have chosen a bacterial expression system to synthesize the EAV nsp10 protein in sufficient amounts for enzymatic studies. The nsp10 sequence was amino terminally fused to the MBP of *E. coli*, which allowed for the purification

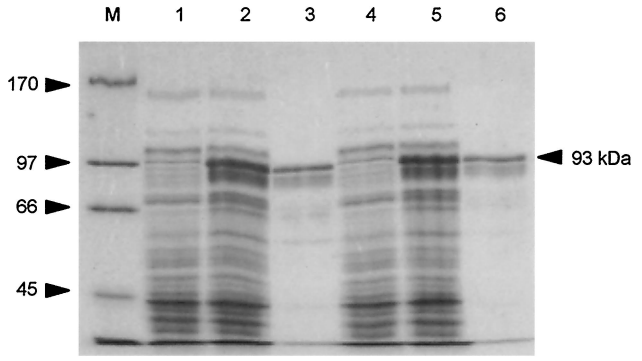

FIG. 1. Purification of MBP-nsp10 and MBP-nsp10-KQ from *E. coli* lysates. The MBP fusion proteins were purified by affinity chromatography as described in Materials and Methods. An SDS–10% polyacrylamide gel stained with Coomassie brilliant blue dye is shown, and the position of the recombinant 93-kDa proteins is indicated by an arrowhead. Lanes: M, protein molecular mass markers (with masses, in kilodaltons, indicated on the left); 1, total lysate from *E. coli* cells transformed with pMal-nsp10; 2, total lysate from IPTG-induced *E. coli* cells transformed with pMal-nsp10; 3, 3 μg of amylose affinity-purified MBP-nsp10 protein; 4, total lysate from *E. coli* cells transformed with pMal-nsp10-KQ; 5, total lysate from IPTG-induced *E. coli* cells transformed with pMal-nsp10-KQ; 6, 3 μg of amylose affinity-purified MBP-nsp10-KQ protein.

of the MBP-nsp10 fusion protein by amylose affinity chromatography. Also, a mutant protein of MBP-nsp10 was produced in which Gln was substituted for the Walker A box (59) Lys-2534 residue of the EAV ORF1ab protein. This control protein was called MBP-nsp10-KQ. It should be noted that, in the context of the infectious EAV cDNA clone (53), this Lys-to-Gln substitution in nsp10 has proven to completely abolish viral RNA synthesis (L. C. van Dinten and E. J. Snijder, unpublished data). The expression of the recombinant proteins was analyzed by SDS-polyacrylamide gel electrophoresis and Western blotting. After induction of recombinant protein expression with IPTG, lysates from both TB1(pMal-nsp10) and TB1(pMal-nsp10-KQ) cells contained an abundant protein that was absent in lysates from noninduced cells (Fig. 1, lanes 1, 2, 4, and 5). The migration of the IPTG-induced proteins in SDS gels corresponded well to the calculated molecular masses of the MBP-nsp10 and MBP-nsp10-KQ fusion proteins (93 kDa). The identity of the recombinant fusion proteins was unequivocally confirmed by Western blotting using the nsp10-specific rabbit antiserum αB2 (data not shown), which recognizes the amino acids 2812 through 2827 of the EAV ORF1ab protein (56). The Western blot data also revealed a slight intracellular degradation of both MBP-nsp10 and MBP-nsp10-KQ (data not shown). Obviously, some degradation products have been copurified by the amylose affinity purification procedure used in this study (Fig. 1, lanes 3 and 6). Protein expression at 24°C provided sufficient amounts of soluble protein and thus allowed the use of a nondenaturing-purification protocol (Fig. 1, lanes 3 and 6). Routinely, about 6 mg of partially purified protein was obtained from a 400-ml culture volume. Attempts to release the authentic EAV nsp10 domain from MBP by endoproteinase Xa treatment failed; even after prolonged incubation, only minor portions of the fusion proteins were cleaved. Nevertheless, since a number of helicases have proven to be enzymatically active as MBP fusion proteins (4, 23, 43), we decided to use the intact fusion proteins for further biochemical analysis.

MBP-nsp10 has ATPase and GTPase activities that are strongly stimulated by specific types of polynucleotides. We first used the MBP-nsp10 protein to examine its predicted ATPase activity. In the experiment shown in Fig. 2, we were able to demonstrate that ATP is hydrolyzed by MBP-nsp10, albeit with low efficacy. However, if the assay was done in the presence of 1 or 150 μg of poly(U) per ml (Fig. 2, lanes 4 and 5, respectively), a strong stimulation of the ATPase activity of MBP-nsp10 was observed. In contrast, if either the MBP-nsp10-KQ protein or no protein at all was used, nearly no ATP hydrolysis was detectable. These data clearly support the presumed but never demonstrated ATPase activity of nsp10. The apparent lack of ATPase activity in the MBP-nsp10-KQ protein suggests an indispensability of Lys-2534 for nsp10 activity. This result is consistent with previous mutagenesis studies that have implicated equivalent Lys residues of the Walker A motif in the function of numerous helicase-associated NTPase activities (reviewed in 20). Furthermore, it strongly suggests that the observed ATPase activity is mediated by MBP-nsp10 rather than any impurity of the preparations and that MBP-nsp10-KQ would be an appropriate control in subsequent experiments.

An additional set of experiments revealed that MBP-nsp10 hydrolyzed ATP and GTP with comparable efficacies (data not shown) and that the nsp10 NTPase activity depends on the presence of divalent cations. Thus, no NTPase activity was detected if the reaction lacked magnesium ions or if EDTA was added in millimolar amounts (data not shown). Divalent cations have also been shown to be required in many other helicase-associated NTPase activities (32).

Stimulation of NTPase activity by nucleic acids is an intrinsic property of most helicases (32), and our initial poly(U) stimulation data (see above) suggested that this may also be the case for the nsp10 NTPase activity. We therefore examined the effect of different DNA and RNA polynucleotides on the ATPase activity of MBP-nsp10 in more detail (Table 1). The assays were done in buffer N containing 600 fmol of MBP-nsp10. The reactions also contained 2 mM sodium chloride that originated from the protein storage buffer. ATP hydrolysis was measured by phosphorimaging of the reaction products following thin-layer chromatography. The ATPase activity in the absence of polynucleotides was taken to be 1.0, and all other activities were normalized to this value. Also, the data were collected prior to 20% substrate depletion to obtain initial hydrolysis velocities. The data summarized in Table 1 show

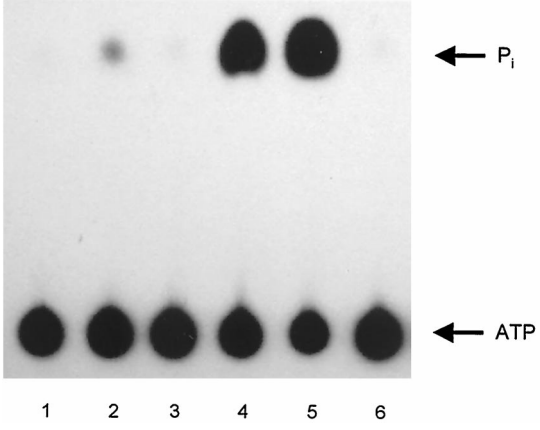

FIG. 2. ATPase activity of MBP-nsp10. The ATPase activity was analyzed by thin-layer chromatography using [γ-^{32}P]ATP as a substrate as described in Materials and Methods. The positions of ATP and inorganic phosphate (P_i) are indicated. Lanes: 1, reaction without protein; 2, reaction containing 600 fmol of MBP-nsp10; 3, reaction containing 600 fmol of MBP-nsp10-KQ; 4, reaction containing 600 fmol of MBP-nsp10 and 1 μg of poly(U) per ml; 5, reaction containing 600 fmol of MBP-nsp10 and 150 μg of poly(U) per ml; 6, reaction containing 600 fmol of MBP-nsp10-KQ and 150 μg of poly(U) per ml.

TABLE 1. Effect of polynucleotides on the ATPase activity of MBP-nsp10

Polynucleotide	Relative ATPase activity[a]
None	1
Poly(U)	18
Poly(A)	4
Poly(C)	3
Poly(G)	1
tRNA	2
Poly(dT)	20
Poly(dA)	15

[a] The enzymatic activity without added polynucleotides was taken to be 1.0, and all other activities were normalized to this value. Each value represents the average of three independent determinations, which did not vary by more than 20%.

that poly(dA), poly(U), and poly(dT) were the strongest stimulators of the MBP-nsp10-associated ATPase activity with a 15- to 20-fold increase of the basal activity (Table 1). Poly(A), poly(C) and tRNA stimulated the ATPase activity to a lesser extent, and poly(G) was inactive. The calculation of the specific activity of MBP-nsp10 in the presence of the strongest stimulator, poly(dT), revealed that 1 pmol of MBP-nsp10 hydrolyzed 0.5 nmol of ATP per min. The extent of ATPase stimulation by specific polynucleotides is similar to that reported for RNA virus SF2 helicases (27) but stands in sharp contrast to most other RNA virus SF1 helicases, in which stimulatory effects of not more than twofold have been reported (18, 26, 42). The only RNA virus SF1 helicase for which comparably high stimulatory effects of polynucleotides on the ATPase activity have been found is the human coronavirus helicase (46).

Effects of increasing salt concentrations on MBP-nsp10 ATPase activity. Variations of the salt concentration are known to strongly influence the stability and kinetics of protein-nucleic acid interactions (33). Probably an increase in cation concentration decreases the gain of entropy that normally occurs upon cation release during complex formation. To study the effects of varying the salt concentration on both the basal and the poly(U)-stimulated MBP-nsp10 ATPase activity, the extent of ATP hydrolysis at increasing potassium chloride concentrations was determined. In these experiments, the maximal extent of substrate hydrolysis (in the absence of salt) was set to be 50%, which still allowed the reliable detection of strongly reduced ATPase activities at high salt concentrations. Because of the low ATPase activity in the absence of polynucleotides, the reactions without poly(U) were incubated with 4 pmol of MBP-nsp10, whereas the reactions containing poly(U) were incubated with 250 fmol of MBP-nsp10. Due to the transfer of sodium chloride from the protein storage buffer, the reactions contained different amounts of sodium chloride [16 mM NaCl versus 1 mM NaCl in the reactions without and with poly(U), respectively]. The ATPase activity in the absence of potassium chloride was taken to be 100%, and all other activities were normalized to this value. The basal ATPase activity of MBP-nsp10 in the absence of poly(U) was not significantly affected by up to 250 mM potassium chloride concentrations and still retained 80% activity at 500 mM potassium chloride (data not shown). In contrast, the poly(U)-stimulated ATPase activity of MBP-nsp10 proved to be extremely sensitive to increasing salt concentrations. The data summarized in Fig. 3 clearly indicate that monovalent-cation concentrations above 20 to 25 mM significantly inhibited the enzymatic activity.

RNA duplex-unwinding activity of MBP-nsp10. A standard in vitro assay (35) was used to analyze the RNA helicase activity of MBP-nsp10. The test substrates consisted of two partially complementary RNA strands of which one was radiolabeled. The substrates were incubated with MBP-nsp10 and the ATPase-deficient MBP-nsp10-KQ protein, respectively, in a buffer containing ATP and magnesium. The separation of the partial-duplex substrate into single-stranded reaction products was examined by nondenaturing gel electrophoresis.

Helicases bind to the single-stranded tail of their partial-duplex substrates with a specific orientation with respect to the polarity of the sugar-phosphate backbone. This property determines the directionality (or polarity) of the duplex-unwinding reaction and allows for the classification into 3′-to-5′ helicases and 5′-to-3′ helicases (32). In a first set of experiments, we used partial-duplex RNA substrates carrying different single-stranded regions. The first substrate, 5′-RNA2, consisted of a 22-nucleotide (nt) duplex and two 5′ single-stranded regions of 21 and 7 nt at opposite ends of the substrate. The 21-nt tail essentially consisted of oligo(U). The second substrate, 3′-RNA2, also contained a 22-nt duplex region, but had a 3′-single-stranded region, consisting of oligo(U)$_{15}$. Substrates incubated with buffer (Fig. 4, lanes 1 and 6) as well as heat-denatured substrates (Fig. 4, lanes 2 and 7) were used as size markers to localize the duplex RNA substrates and the displaced, radiolabeled single-stranded RNA products. As Fig. 4 shows, MBP-nsp10 was able to unwind the 5′-tailed 5′-RNA2 (lane 4) but not the 3′-tailed 3′-RNA2 (lane 9). The helicase activity required the presence of ATP (Fig. 4, cf. lanes 3 and 4) or GTP (data not shown), which is consistent with previous results showing that helicase-catalyzed unwinding of nucleic acids is an energy-dependent process (31, 35). Accordingly, the NTPase-deficient control protein MBP-nsp10-KQ completely lacked helicase activity (Fig. 4, lanes 5 and 10). The combined data led us to conclude that the MBP-nsp10 protein has RNA duplex-unwinding activity and operates with 5′-to-3′ polarity.

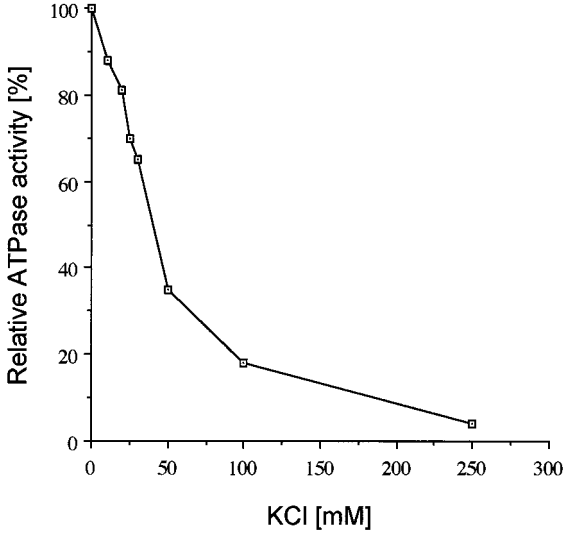

FIG. 3. Effect of increasing monovalent-cation concentration on the poly(U)-stimulated ATPase activity of MBP-nsp10. The ATPase activity was analyzed by thin-layer chromatography using [γ-^{32}P]ATP as a substrate as described in Materials and Methods and quantified by phosphorimaging. The poly(U)-stimulated ATPase activity in the absence of potassium chloride was taken to be 100%, and all other activities were normalized to this value (see text for details).

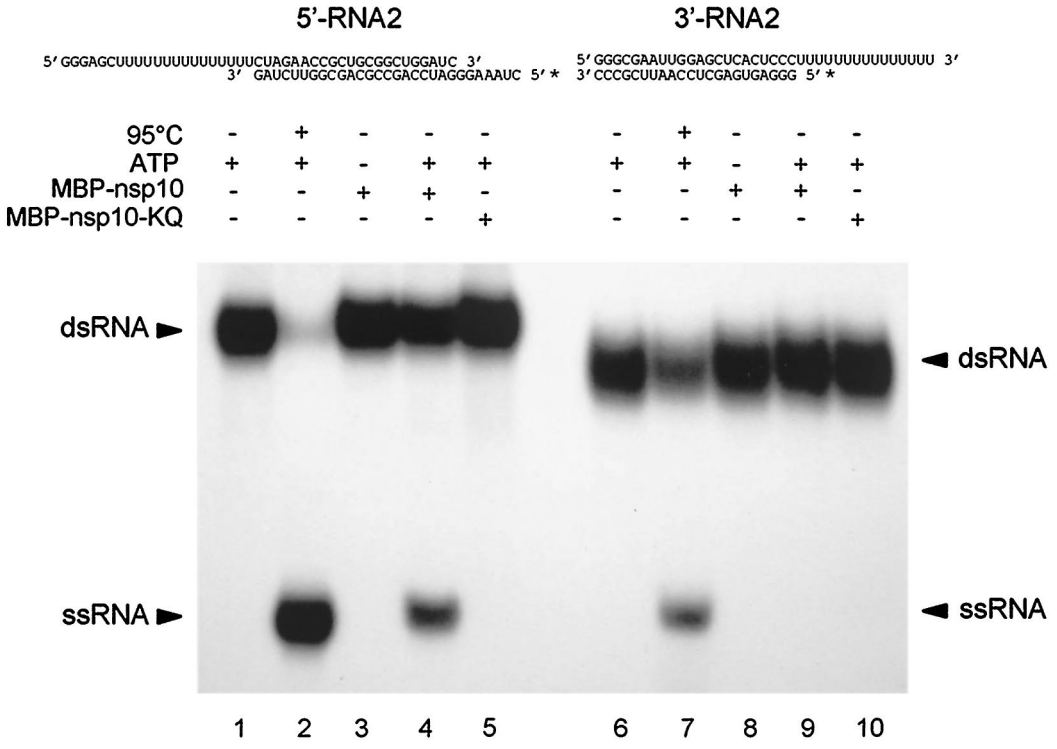

FIG. 4. MBP-nsp10 5′-to-3′ RNA duplex-unwinding activity. Reaction conditions were as described in Materials and Methods with approximately 90 fmol of RNA substrate per reaction. The structures of the substrates are shown schematically with the radiolabeled strands marked by asterisks. The reaction products were separated on nondenaturing, 10 to 20% gradient polyacrylamide gels. The positions of the partially double-stranded substrates (dsRNA) and the displaced monomeric products (ssRNA) are indicated. Lanes: 1, incubation of 5′-RNA2 without protein; 2, heat-denatured 5′RNA2; 3, incubation of 5′-RNA2 with 3 pmol of MBP-nsp10 in the absence of ATP; 4, incubation of 5′-RNA2 with 3 pmol of MBP-nsp10 in the presence of 5 mM ATP; 5, incubation of 5′-RNA2 with 3 pmol of MBP-nsp10-KQ in the presence of 5 mM ATP; 6, incubation of 3′-RNA2 without protein; 7, heat-denatured 3′-RNA2; 8, incubation of 3′-RNA2 with 3 pmol of MBP-nsp10 in the absence of ATP; 9, incubation of 3′-RNA2 with 3 pmol of MBP-nsp10 in the presence of 5 mM ATP; 10, incubation of 3′-RNA2 with 3 pmol of MBP-nsp10-KQ in the presence of 5 mM ATP.

DNA duplex-unwinding activity of MBP-nsp10. As shown in Table 1, the ATPase activity of MBP-nsp10 was strongly stimulated by the DNA homopolymers poly(dT) and poly(dA). These data prompted us to analyze the unwinding activity of MBP-nsp10 on duplex DNA substrates. The DNA substrates we used had identical 22-bp duplex regions to which (except for the completely double-stranded substrate DNA-0) 30-nt-long, single-stranded oligo(dT) tails were attached at different positions.

The data presented in Fig. 5 show that MBP-nsp10 was able to unwind substrates containing 5′ single-stranded tails alone or in combination with 3′ single-stranded tails, irrespective of whether they were present on the same end or on opposite ends of the substrate (Fig. 5, lanes 7, 11, and 19). In contrast, if the DNA substrates contained only a 3′ tail or no single-stranded tail, they were not unwound by MBP-nsp10 (Fig. 5, lanes 3 and 15). As expected, the ATPase-deficient MBP-nsp10-KQ protein was not able to unwind any of the substrates (Fig. 5, lanes 4, 8, 12, 16, and 20).

The forked substrate 5′-3′-DNA-T30, which carries 5′ and 3′ single-stranded tails on the same end of the duplex, appeared to be more readily unwound by MBP-nsp10 than the substrates 5′-DNA-3′-T30 and 5′-DNA-T30 (Fig. 5, cf. lanes 7, 11, and 19). To determine whether this substrate is indeed more readily unwound by MBP-nsp10 or, alternatively, whether different reannealing kinetics are responsible for the observed difference, we analyzed the reannealing kinetics of the DNA substrates 5′-3′-DNA-T30 and 5′-DNA-T30 after strand separation. To this end, both DNA substrates were denatured (95°C, 5 min) and subsequently placed on ice for 10 min. The denatured substrates were then subjected to a standard helicase assay without MBP-nsp10, and the reaction products were analyzed by nondenaturing gel electrophoresis. Quantitation of the double-stranded and single-stranded forms of the two substrates by phosphorimaging revealed that 90% of the DNA substrate 5′-3′-DNA-T30 but only 75% of DNA substrate 5′-DNA-T30 had remained single stranded (data not shown). We concluded from this experiment that substrate 5′-DNA-T30 reanneals more rapidly than the twin-tailed 5′-3′-DNA-T30. We therefore consider it likely that the apparently incomplete unwinding of the 5′-DNA-3′-T30 and 5′-DNA-T30 substrates reflects a rapid reannealing of the separated strands rather than a low activity of MBP-nsp10 on these substrates.

In summary, the data suggest that the DNA duplex-unwinding activity strictly depends on the presence of 5′ single-stranded tails, which again supports the conclusion that EAV nsp10 is a helicase with 5′-to-3′ polarity.

DISCUSSION

Although more than a decade ago a large number of RNA virus families were predicted to encode SF1 helicases (13, 16), no convincing evidence for duplex-unwinding activity has been obtained for most of these proteins. Therefore, their functional assignment as true helicases has been questioned, and alternative functions have been considered for these proteins (27). The identification of duplex-unwinding activities for three of these proteins, the Semliki Forest virus nsp2 protein (11), the

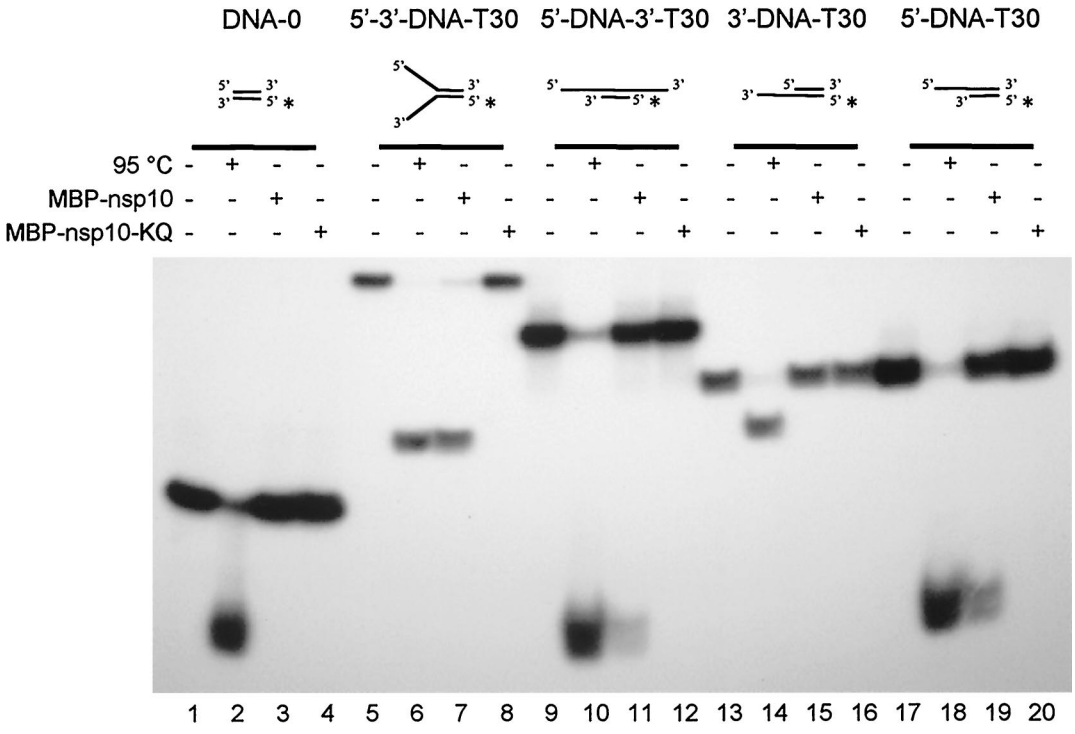

FIG. 5. MBP-nsp10 5′-to-3′ DNA duplex-unwinding activity. Reaction conditions were as described in Materials and Methods with approximately 25 fmol of DNA substrates per reaction. The structures of the substrates are shown schematically with the radiolabeled strands marked by asterisks. With the exception of DNA-0, which was entirely double-stranded, the substrates consisted of identical 22-bp duplexes to which 30-nt-long, single-stranded oligo(dT) tails were attached at different positions. The reaction products were separated on nondenaturing, 10 to 20% gradient polyacrylamide gels. Lanes: 1, 5, 9, 13, and 17, reactions without protein; 2, 6, 10, 14, and 18, heat-denatured DNA substrates; 3, 7, 11, 15, and 19, reactions containing 2 pmol of MBP-nsp10; 4, 8, 12, 16, and 20, reactions containing 2 pmol of MBP-nsp10-KQ.

HCoV helicase (46), and the EAV nsp10 (this study), provides clear biochemical evidence for the early sequence-based predictions and strongly suggests that other RNA virus helicases of SF1 may also represent duplex-unwinding enzymes. The recently observed preference of the HCoV helicase for pyrimidine-tailed substrates (46), however, supports the idea that at least some of these proteins may require specific substrates to display their helicase activities.

The characterization of its ATPase and helicase activities revealed that nsp10 shares a number of biochemical properties with the HCoV helicase. First, and probably most importantly, nsp10 and the HCoV helicase share a 5′-to-3′ polarity in their unwinding reactions, whereas all RNA virus SF2 enzymes analyzed to date operate in 3′-to-5′ direction (reviewed in 27). This finding implies that nidovirus helicases bind to the 5′ single-stranded region of a partial duplex RNA and unwind this duplex in a 5′-to-3′ direction with respect to the RNA strand used for entry. Even though the 5′-to-3′ polarity has now been demonstrated for two RNA viral enzymes of SF1, it is certainly premature to propose a 5′-to-3′ polarity for all RNA virus SF1 helicases. In this respect, it should be kept in mind that there are many cellular and DNA virus SF1 helicases with proven 3′-to-5′ directionality (15). Also, recent studies on molecular motors of the kinesin superfamily have shown that the specific arrangement of a motor domain and its associated accessory domain(s) (rather than the intrinsic properties of the motor domain itself) determines the polarity of translocation (21), and it has been speculated that this model may also apply to the function of helicases (2).

Second, both proteins were strongly stimulated by a nearly identical range of polynucleotides, with poly(U), poly(dT), and poly(dA) being the most active cofactors. In contrast, none of the enzymes was stimulated by poly(G). The levels of stimulation were surprisingly high in both enzymes (up to 50-fold in the HCoV helicase and up to 20-fold in nsp10). Thus, the values substantially surpassed the stimulatory effects reported for the ATPase activities of other RNA virus SF1 helicases (18, 26, 42). The stimulation of the ATPase activity upon binding to single-stranded nucleic acid most likely reflects a conformational change in nsp10, stabilizing the bound ATP molecule in a conformation that is required for rapid hydrolysis. This conformational change has long been proposed to occur in most NTPases, and recently it was indeed verified by structural data (51). The poly(U)-stimulated ATPase activity of nsp10 proved to be extremely sensitive to increasing salt concentrations. Similar results have also been obtained for other virus-encoded, helicase-associated NTPase activities (10, 60, 61). At least in some cases, direct evidence was obtained to show that, even in the presence of very low concentrations of monovalent cations, the binding of a given enzyme to nucleic acid was significantly reduced (10). The fact that the basal NTPase activity of nsp10 was not significantly affected by moderate salt concentrations (up to 250 mM) suggests that the overall conformation of nsp10 was maintained at this ionic strength. We therefore interpret the data to show that monovalent cations interfere with the binding of nsp10 to its nucleic acid cofactor, which, in turn, prevents the enzyme from assuming the specific conformation required for effective ATP hydrolysis. Since the physiological ionic strength in the cytoplasm is about 150 mM, it is likely that the functionality of nsp10 in vivo is maintained by a specific microenvironment. Nsp10 has been shown to be part of the viral replication complex (56), and it is conceivable that

specific protein-protein interactions in conjunction with membranes may exclude salt from the immediate environment of the helicase or change the salt sensitivity of the enzyme.

Third, it appears that the substrate-binding pockets of both nsp10 and the HCoV helicase do not significantly discriminate between RNA and DNA. This conclusion is supported by the observation that both RNA and DNA homopolymers were able to stimulate the ATPase activities of nsp10 and the HCoV helicase. Similarly, both RNA and DNA duplexes are readily unwound by the two enzymes. The nidovirus enzymes share this lack of specificity with only a few other helicases (1, 19, 28, 45, 62), whereas the majority of helicases act very specifically on either DNA or RNA.

It should be noted here that the similarity between the EAV and HCoV helicases is not restricted to their common biochemical properties. There are additional peculiarities that support a close phylogenetic and functional relationship between these enzymes. First, both the arterivirus and the coronavirus helicases are localized downstream of the polymerase domain in the viral polyprotein, an arrangement that is extremely unusual among positive-strand RNA viruses, where the helicase generally precedes the polymerase domain (29). Second, both the arterivirus and the coronavirus helicases are combined with supergroup 1 polymerases, whereas all other RNA viral SF1 helicases are combined with polymerases of supergroup 3 (29). And third, both enzymes use a combination of an amino-terminal Zn finger domain and a downstream SF1 helicase domain (6, 7, 17, 23, 56). Taken together, these observations lead us to suggest that the two nidovirus proteins are closely related and can be expected to have similar functions in the virus life cycle. Also, the data provide additional support for a common ancestry of the nidovirus replicase genes as previously postulated on the basis of sequence comparison data (6). Obviously, the conserved 5′-to-3′ polarity of the arteri- and coronavirus helicases stands in contrast to the 3′-to-5′ polarity of RNA virus SF2 helicases, suggesting that the nidovirus enzymes may have functions that fundamentally differ from the distantly related SF2 helicases of the poty-, flavi- and pestilike viruses.

In the EAV reverse genetic system (53), it has recently been demonstrated that the nsp10-associated Zn finger domain is a multifunctional protein that is specifically involved in such different processes as genome replication, sg mRNA transcription, and virion biogenesis (55). The bacterial expression system described in this study can be expected to provide a valuable tool in the functional and, possibly, structural characterization of nsp10. Furthermore, the in vitro DNA helicase activity of nsp10 allows for the use of DNA substrates and will thus greatly facilitate the detailed analysis of the substrate specificity of nsp10. Obviously, one of our primary goals will be to examine the functional relevance of the Zn finger structure and the hinge spacer region, which connects the Zn finger and the helicase domain, to the enzymatic activities of nsp10. As a first step towards this goal, mutant forms of nsp10 will be characterized, and we hope that, in combination with the in vivo data reported recently (55), these studies will provide clues to the understanding of the physical interactions between the individual subdomains of nsp10.

ACKNOWLEDGMENTS

The work of Anja Seybert was supported by grants from the Deutsche Forschungsgemeinschaft (SI 357/4-1) and the Fonds der Chemischen Industrie (FCI).

We thank Jessika Dobbe for technical support and gratefully acknowledge Alexander E. Gorbalenya for helpful discussions during the course of these studies.

REFERENCES

1. **Bayliss, C. D., and G. L. Smith.** 1996. Vaccinia virion protein I8R has both DNA and RNA helicase activities: implications for vaccinia virus transcription. J. Virol. **70:**794–800.
2. **Bird, L. E., H. S. Subramanya, and D. B. Wigley**. 1998. Helicases: a unifying structural theme? Curr. Opin. Struct. Biol. **8:**14–18.
3. **Cavanagh, D.** 1997. Nidovirales: a new order comprising Coronaviridae and Arteriviridae. Arch. Virol. **142:**629–633.
4. **Chiorini, J. A., M. D. Weitzman, R. A. Owens, E. Urcelay, B. Safer, and R. M. Kotin.** 1994. Biologically active Rep proteins of adeno-associated virus type 2 produced as fusion proteins in *Escherichia coli.* J. Virol. **68:**797–804.
5. **Dé, I., S. G. Sawicki, and D. L. Sawicki.** 1996. Sindbis virus RNA-negative mutants that fail to convert from minus-strand to plus-strand synthesis: role of the nsP2 protein. J. Virol. **70:**2706–2719.
6. **den Boon, J. A., E. J. Snijder, E. D. Chirnside, A. A. de Vries, M. C. Horzinek, and W. J. Spaan.** 1991. Equine arteritis virus is not a togavirus but belongs to the coronaviruslike superfamily. J. Virol. **65:**2910–2920.
7. **Denison, M. R., W. J. Spaan, Y. van der Meer, C. A. Gibson, A. C. Sims, E. Prentice, and X. T. Lu.** 1999. The putative helicase of the coronavirus mouse hepatitis virus is processed from the replicase gene polyprotein and localizes in complexes that are active in viral RNA synthesis. J. Virol. **73:**6862–6871.
8. **de Vries, A. A. F., M. C. Horzinek, P. J. M. Rottier, and R. J. de Groot.** 1997. The genome organization of the Nidovirales: similarities and differences between arteri, toro-, and coronaviruses. Semin. Virol. **8:**33–47.
9. **Dracheva, S., E. V. Koonin, and J. J. Crute.** 1995. Identification of the primase active site of the herpes simplex virus type 1 helicase-primase. J. Biol. Chem. **270:**14148–14153.
10. **Eagles, R. M., E. Balmori-Melian, D. L. Beck, R. C. Gardner, and R. L. Forster.** 1994. Characterization of NTPase, RNA-binding and RNA-helicase activities of the cytoplasmic inclusion protein of tamarillo mosaic potyvirus. Eur. J. Biochem. **224:**677–684.
11. **Gomez de Cedrón, M., N. Ehsani, M. L. Mikkola, J. A. García, and L. Kääriäinen.** 1999. RNA helicase activity of Semliki Forest virus replicase protein NSP2. FEBS Lett. **448:**19–22.
12. **Gorbalenya, A. E., V. M. Blinov, A. P. Donchenko, and E. V. Koonin.** 1989. An NTP-binding motif is the most conserved sequence in a highly diverged monophyletic group of proteins involved in positive strand RNA viral replication. J. Mol. Evol. **28:**256–268.
13. **Gorbalenya, A. E., and E. V. Koonin.** 1989. Viral proteins containing the purine NTP-binding sequence pattern. Nucleic Acids Res. **17:**8413–8440.
14. **Gorbalenya, A. E., and E. V. Koonin.** 1993. Comparative analysis of amino-acid sequences of key enzymes of replication and expression of positive-strand RNA viruses. Validity of approach and functional and evolutionary implications. Sov. Sci. Rev. D. Physicochem. Biol. **11:**1–84.
15. **Gorbalenya, A. E., and E. V. Koonin.** 1993. Helicases: amino acid sequence comparisons and structure-function relationships. Curr. Opin. Struct. Biol. **3:** 419–429.
16. **Gorbalenya, A. E., E. V. Koonin, A. P. Donchenko, and V. M. Blinov.** 1988. A novel superfamily of nucleoside triphosphate-binding motif containing proteins which are probably involved in duplex unwinding in DNA and RNA replication and recombination. FEBS Lett. **235:**16–24.
17. **Gorbalenya, A. E., E. V. Koonin, A. P. Donchenko, and V. M. Blinov.** 1989. Coronavirus genome: prediction of putative functional domains in the nonstructural polyprotein by comparative amino acid sequence analysis. Nucleic Acids Res. **17:**4847–4861.
18. **Gros, C., and G. Wengler.** 1996. Identification of an RNA-stimulated NTPase in the predicted helicase sequence of the Rubella virus nonstructural polyprotein. Virology **217:**367–372.
19. **Gwack, Y., D. W. Kim, J. H. Han, and J. Choe.** 1997. DNA helicase activity of the hepatitis C virus nonstructural protein 3. Eur. J. Biochem. **250:**47–54.
20. **Hall, M. C., and S. W. Matson.** 1999. Helicase motifs: the engine that powers DNA unwinding. Mol. Microbiol. **34:**867–877.
21. **Henningsen, U., and M. Schliwa.** 1997. Reversal in the direction of movement of a molecular motor. Nature **389:**93–96.
22. **Herold, J., S. Siddell, and J. Ziebuhr.** 1996. Characterization of coronavirus RNA polymerase gene products. Methods Enzymol. **275:**68–89.
23. **Heusipp, G., U. Harms, S. G. Siddell, and J. Ziebuhr.** 1997. Identification of an ATPase activity associated with a 71-kilodalton polypeptide encoded in gene 1 of the human coronavirus 229E. J. Virol. **71:**5631–5634.
24. **Janda, M., and P. Ahlquist.** 1998. Brome mosaic virus RNA replication protein 1a dramatically increases in vivo stability but not translation of viral genomic RNA3. Proc. Natl. Acad. Sci. USA **95:**2227–2232.
25. **Johnson, R. E., S. T. Henderson, T. D. Petes, S. Prakash, M. Bankmann, and L. Prakash.** 1992. Saccharomyces cerevisiae RAD5-encoded DNA repair protein contains DNA helicase and zinc-binding sequence motifs and affects the stability of simple repetitive sequences in the genome. Mol. Cell. Biol. **12:** 3807–3818.
26. **Kadaré, G., C. David, and A. L. Haenni.** 1996. ATPase, GTPase, and RNA binding activities associated with the 206-kilodalton protein of turnip yellow mosaic virus. J. Virol. **70:**8169–8174.
27. **Kadaré, G., and A. L. Haenni.** 1997. Virus-encoded RNA helicases. J. Virol. **71:**2583–2590.

28. **Kim, H. D., J. Choe, and Y. S. Seo.** 1999. The sen1(+) gene of Schizosaccharomyces pombe, a homologue of budding yeast SEN1, encodes an RNA and DNA helicase. Biochemistry **38:**14697–14710.
29. **Koonin, E. V., and V. V. Dolja.** 1993. Evolution and taxonomy of positive-strand RNA viruses: implications of comparative analysis of amino acid sequences. Crit. Rev. Biochem. Mol. Biol. **28:**375–430.
30. **Kroner, P. A., B. M. Young, and P. Ahlquist.** 1990. Analysis of the role of brome mosaic virus 1a protein domains in RNA replication, using linker insertion mutagenesis. J. Virol. **64:**6110–6120.
31. **Lohman, T. M.** 1993. Helicase-catalyzed DNA unwinding. J. Biol. Chem. **268:**2269–2272.
32. **Lohman, T. M., and K. P. Bjornson.** 1996. Mechanisms of helicase-catalyzed DNA unwinding. Annu. Rev. Biochem. **65:**169–214.
33. **Lohman, T. M., and D. P. Mascotti.** 1992. Thermodynamics of ligand-nucleic acid interactions. Methods Enzymol. **212:**400–424.
34. **Mannhaupt, G., R. Stucka, S. Ehnle, I. Vetter, and H. Feldmann.** 1992. Molecular analysis of yeast chromosome II between CMD1 and LYS2: the excision repair gene RAD16 located in this region belongs to a novel group of double-finger proteins. Yeast **8:**397–408.
35. **Matson, S. W., and K. A. Kaiser-Rogers.** 1990. DNA helicases. Annu. Rev. Biochem. **59:**289–329.
36. **O'Reilly, E. K., N. Tang, P. Ahlquist, and C. C. Kao.** 1995. Biochemical and genetic analyses of the interaction between the helicase-like and polymerase-like proteins of the brome mosaic virus. Virology **214:**59–71.
37. **O'Reilly, E. K., Z. Wang, R. French, and C. C. Kao.** 1998. Interactions between the structural domains of the RNA replication proteins of plant-infecting RNA viruses. J. Virol. **72:**7160–7169.
38. **Osman, T. A., and K. W. Buck.** 1996. Complete replication in vitro of tobacco mosaic virus RNA by a template-dependent, membrane-bound RNA polymerase. J. Virol. **70:**6227–6234.
39. **Ouzounis, C. A., and B. J. Blencowe.** 1991. Bacterial DNA replication initiation factor priA is related to proteins belonging to the 'DEAD-box' family. Nucleic Acids Res. **19:**6953.
40. **Pedersen, K. W., Y. van der Meer, N. Roos, and E. J. Snijder.** 1999. Open reading frame 1a-encoded subunits of the arterivirus replicase induce endoplasmic reticulum-derived double-membrane vesicles which carry the viral replication complex. J. Virol. **73:**2016–2026.
41. **Petty, I. T., R. French, R. W. Jones, and A. O. Jackson.** 1990. Identification of barley stripe mosaic virus genes involved in viral RNA replication and systemic movement. EMBO J. **9:**3453–3457.
42. **Rikkonen, M., J. Peränen, and L. Kääriäinen.** 1994. ATPase and GTPase activities associated with Semliki Forest virus nonstructural protein nsP2. J. Virol. **68:**5804–5810.
43. **Rodriguez, P. L., and L. Carrasco.** 1993. Poliovirus protein 2C has ATPase and GTPase activities. J. Biol. Chem. **268:**8105–8110.
44. **Rouleau, M., R. J. Smith, J. B. Bancroft, and G. A. Mackie.** 1994. Purification, properties, and subcellular localization of foxtail mosaic potexvirus 26-kDa protein. Virology **204:**254–265.
45. **Scheffner, M., R. Knippers, and H. Stahl.** 1989. RNA unwinding activity of SV40 large T antigen. Cell **57:**955–963.
46. **Seybert, A., A. Hegyi, S. G. Siddell, and J. Ziebuhr.** 2000. The human coronavirus 229E superfamily 1 helicase has RNA and DNA duplex-unwinding activities with 5′-to-3′ polarity. RNA **6:**1056–1068.
47. **Snijder, E. J., and J. J. Meulenberg.** 1998. The molecular biology of arteriviruses. J. Gen. Virol. **79:**961–979.
48. **Snijder, E. J., A. L. Wassenaar, and W. J. Spaan.** 1992. The 5′ end of the equine arteritis virus replicase gene encodes a papainlike cysteine protease. J. Virol. **66:**7040–7048.
49. **Snijder, E. J., A. L. Wassenaar, W. J. Spaan, and A. E. Gorbalenya.** 1995. The arterivirus nsp2 protease: an unusual cysteine protease with primary structure similarities to both papain-like and chymotrypsin-like proteases. J. Biol. Chem. **270:**16671–16676.
50. **Snijder, E. J., A. L. Wassenaar, L. C. van Dinten, W. J. Spaan, and A. E. Gorbalenya.** 1996. The arterivirus nsp4 protease is the prototype of a novel group of chymotrypsin-like enzymes, the 3C-like serine proteases. J. Biol. Chem. **271:**4864–4871.
51. **Soultanas, P., M. S. Dillingham, S. S. Velankar, and D. B. Wigley.** 1999. DNA binding mediates conformational changes and metal ion coordination in the active site of PcrA helicase. J. Mol. Biol. **290:**137–148.
52. **van der Meer, Y., H. van Tol, J. Krijnse Locker, and E. J. Snijder.** 1998. ORF1a-encoded replicase subunits are involved in the membrane association of the arterivirus replication complex. J. Virol. **72:**6689–6698.
53. **van Dinten, L. C., J. A. den Boon, A. L. Wassenaar, W. J. Spaan, and E. J. Snijder.** 1997. An infectious arterivirus cDNA clone: identification of a replicase point mutation that abolishes discontinuous mRNA transcription. Proc. Natl. Acad. Sci. USA **94:**991–996.
54. **van Dinten, L. C., S. Rensen, A. E. Gorbalenya, and E. J. Snijder.** 1999. Proteolytic processing of the open reading frame 1b-encoded part of arterivirus replicase is mediated by nsp4 serine protease and is essential for virus replication. J. Virol. **73:**2027–2037.
55. **van Dinten, L. C., H. van Tol, A. E. Gorbalenya, and E. J. Snijder.** 2000. The predicted metal-binding region of the arterivirus helicase protein is involved in subgenomic mRNA synthesis, genome replication, and virion biogenesis. J. Virol. **74:**5213–5223.
56. **van Dinten, L. C., A. L. Wassenaar, A. E. Gorbalenya, W. J. Spaan, and E. J. Snijder.** 1996. Processing of the equine arteritis virus replicase ORF1b protein: identification of cleavage products containing the putative viral polymerase and helicase domains. J. Virol. **70:**6625–6633.
57. **van Marle, G., L. C. van Dinten, W. J. Spaan, W. Luytjes, and E. J. Snijder.** 1999. Characterization of an equine arteritis virus replicase mutant defective in subgenomic mRNA synthesis. J. Virol. **73:**5274–5281.
58. **Visse, R., M. de Ruijter, M. Ubbink, J. A. Brandsma, and P. van de Putte.** 1993. The first zinc-binding domain of UvrA is not essential for UvrABC-mediated DNA excision repair. Mutat. Res. **294:**263–274.
59. **Walker, J. E., M. Saraste, M. J. Runswick, and N. J. Gay.** 1982. Distantly related sequences in the alpha- and beta-subunits of ATP synthase, myosin, kinases and other ATP-requiring enzymes and a common nucleotide binding fold. EMBO J. **1:**945–951.
60. **Wardell, A. D., W. Errington, G. Ciaramella, J. Merson, and M. J. McGarvey.** 1999. Characterization and mutational analysis of the helicase and NTPase activities of hepatitis C virus full-length NS3 protein. J. Gen. Virol. **80:**701–709.
61. **Warrener, P., J. K. Tamura, and M. S. Collett.** 1993. RNA-stimulated NTPase activity associated with yellow fever virus NS3 protein expressed in bacteria. J. Virol. **67:**989–996.
62. **Zhang, S., and F. Grosse.** 1994. Nuclear DNA helicase II unwinds both DNA and RNA. Biochemistry **33:**3906–3912.
63. **Ziebuhr, J., E. J. Snijder, and A. E. Gorbalenya.** 2000. Virus-encoded proteinases and proteolytic processing in the Nidovirales. J. Gen. Virol. **81:**853–879.